JIMA Vol. 73, No. 5 (Dec. 2021) pp. 215-226.

Original

Quantitative assessment of susceptibility artifacts produced by titanium alloy cerebral aneurysm clips on 7 tesla magnetic resonance images

Shouta TSUTSUI [1], Tsuyoshi MATSUDA [2], Kota TAKEDA [2], Makoto SASAKI [2], Kentaro FUJIMOTO [1], Wataru YANAGIHARA [1], Takahiro KOJI [1], Yoshitaka KUBO [1] and Kuniaki OGASAWARA [1]

[1] Department of Neurosurgery, School of Medicine, Iwate Medical University, Yahaba, Japan

[2] Division of Ultrahigh Field MRI, Institute for Biomedical Sciences, Iwate Medical University, Yahaba, Japan

(Received on January 14, 2021 & Accepted on February 12, 2021)

Abstract

Patients with cerebral aneurysms often undergo magnetic resonance imaging (MRI) after microsurgical clipping. The purpose of the present study was to quantitatively assess the magnitudes of susceptibility artifacts produced by various types of titanium alloy aneurysm clip on various sequences of 7 tesla (T) MRI. Five types of titanium alloy aneurysm clip were tested, including combinations of short, long, straight, curved, and fenestrated types. Each clip was placed in a phantom filled with vegetable oil, and was scanned with five different pulse sequences, as follows: three-dimensional (3D) zero time-of-echo (ZTE) imaging; 3D T2-weighted fast spin echo imaging; 3D T1WI with spoiled gradient recalled acquisition in the steady state (SPGR) technique; 3D T2*-weighted with SPGR imaging; and two-dimensional diffusion-weighted imaging. Voxels or pixels containing artifact were determined in each image, and artifact distance and artifact volume were calculated. Susceptibility artifacts were greater on 3D T2*W SPGR than on other sequences and were greater on the long straight clip than other clips. Artifacts on 3D ZTE were less than those on other sequences. Whereas there was prominent development of artifact at both ends, at the curved or fenestrated portion of the clip, artifact was minimal at the mid-part of the blade.

Key words: *susceptibility artifacts, titanium, cerebral aneurysm clip, 7T MRI*

I. Introduction

Patients with cerebral aneurysms often undergo magnetic resonance imaging (MRI) after microsurgical clipping of the aneurysm. Various MRI sequences (e.g., diffusion-weighted imaging [DWI] and magnetic resonance angiography [MRA]) are used to assess the presence of cerebral infarction caused by microsurgical clipping itself or cerebral vasospasm due to subarachnoid hemorrhage [1]. Various MRI sequences are also utilized to detect other intracerebral lesions, including brain tumors, cerebrovascular

Corresponding author: Shouta Tsutsui
stsutsui@iwate-med.ac.jp

disease, or cerebral small vessel disease that can develop many years after microsurgical clipping. MRI at 1.5 tesla (T) and 3T has been used as a primary diagnostic tool in such clinical situations. Ultra-high-field MRI at 7T is becoming clinically available [2]. In particular, this imaging technique provides high diagnostic ability, equal to digital subtraction angiography and superior to lower field MRI for evaluation of micro cerebral aneurysm and aneurysmal dome and neck [2-6].

The most common indication for MRI after microsurgical clipping of an aneurysm is follow-up of the clipped aneurysm and screening for de novo aneurysms [7]. However, cerebral titanium alloy aneurysm clips have safety issues associated with adverse interactions with the static magnetic field (e.g., displacement force and torque) and heating at 7T [8, 9]. In contrast, the results of a phantom study suggested that such clips could be acceptable for 7T examination [8].

Another issue is susceptibility artifacts on the images [10]. Artifacts are produced around the implants and complicate the assessment of lesions [11]. Artifact size generally increases with increasing strength of the static magnetic field. Several investigators demonstrated that the susceptibility artifacts of titanium alloy aneurysm clips on 3T MRI were 1.6 times as high in number as those on 1.5 T MRI [12, 13]. Only one study has assessed the susceptibility artifacts caused by two aneurysm clips including a long straight clip made of cobalt-chrome alloy and a short straight clip made of titanium alloy set in a phantom on gradient-echo sequences at 7T MRI. That study showed that susceptibility artifact of the former clip was greater than that of the latter clip and concluded that the magnitude of the artifact was related to the length of the aneurysm clip [8]. However, a variety of clips, including short, long, straight, curved, and fenestrated types, are widely used in neurosurgical settings and the magnitudes of the susceptibility artifacts have not been compared among the various types.

The purpose of the present study was to quantitatively assess the magnitudes of the susceptibility artifacts produced by various types of titanium alloy aneurysm clip on various sequences of 7T MRI.

II. Materials and Methods

This study was performed according to the American Society for Testing and Materials (ASTM) F2119-07 "Standard Test Method for Evaluation of MR Image Artifacts from Passive Implants" [14].

1. Test Objects

Five types of aneurysm clip were tested, including combinations of short, long, straight, curved, and fenestrated (Fig. 1). All clips were made of titanium alloy (Mizuho, Medical Inc., Tokyo, Japan). Clip length, ordered from shortest to longest, was right-angled type < short straight type < 45°-angled type < straight fenestrated type < long straight type. Clip width, ordered from narrowest to widest, was short straight type = right-angled type = 45° -angled type = straight fenestrated type < long straight type. Clip volume, ordered from lowest to greatest volume, was short straight type < right-angled type < 45° -angled type < straight fenestrated type < long straight type.

2. Phantom

Each aneurysm clip was placed on a web of nylon threads at the center of an acrylic

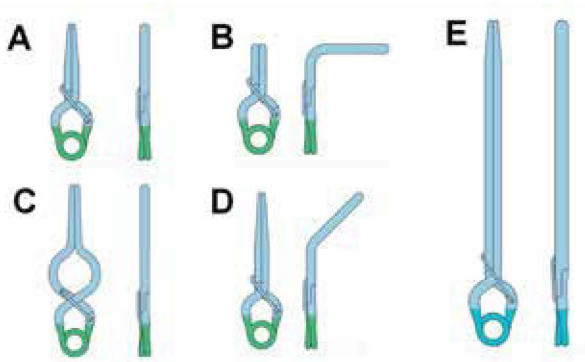

Fig. 1. Schematic drawings of the titanium alloy aneurysm clips tested in the present study. Left, top view; Right, lateral view.
A. 17-001-02: No. 2, short straight type (length, 18.8 mm; width, 5.7 mm; volume, 36.1 mm^3).
B. 17-001-22: No. 22, Right-angled type (length, 15.0 mm; width, 5.7 mm; volume, 49.7 mm^3).
C. 17-001-30: No. 30, straight fenestrated type (length, 24.6 mm; width, 5.7 mm; volume, 57.2 mm^3).
D. 17-001-49: No. 49, 45°-angled type (length, 22.2 mm; width, 5.7 mm; volume, 51.9 mm^3).
E. 17-001-92: No. 92, long straight type (length, 51.5 mm; width, 7.6 mm; volume, 245.3 mm^3).

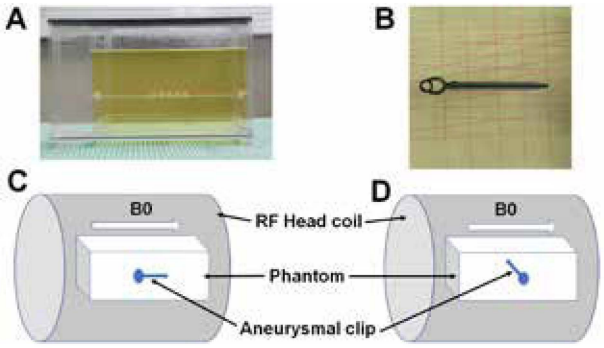

Fig. 2. Photographs and schematic drawings of the phantom and orientations of the clip to the static magnetic field.
A. Lateral view of the acrylic phantom.
B. Top view of an aneurysm clip placed on a web of nylon threads at the center of the phantom.
C. Placement of an aneurysm clip with the long axis oriented parallel to the static magnetic field.
D. Placement of an aneurysm clip with the long axis oriented perpendicular to the static magnetic field.
B0, static magnetic field; RF, radiofrequency.

phantom (height, 14 cm; width, 12 cm; length, 24 cm) that was filled with vegetable oil (Fig. 2 A, B). The ASTM standard protocol F2119-07 recommends using copper sulfate (CuSO4) solution for testing [14]. However, our pilot study revealed nonuniform distribution of signal intensity because the dielectric properties of the CuSO4 solution caused heterogeneous radiofrequency (RF) transmit fields during RF passage through the solution. To avoid this problem, we filled the phantom with vegetable oil, which has low conductivity [15].

3. MR Imaging

MR images were obtained using a 7T MRI system (Discovery MR950, GE Healthcare, Milwaukee, WI, USA) with a 2-channel transmit and 32-channel receive head coil (NM008-32-7GE-MR950, Nova Medical, Wilmington, MA, USA). All aneurysm clips were scanned with each of five different pulse sequences: 3D zero time-of-echo (ZTE) imaging; 3D T2W fast spin echo (FSE) imaging; 3D T1WI with SPGR technique; 3D T2*W with SPGR imaging; two-dimensional (2D) DWI acquired with spin echo (SE) echo planner imaging (EPI). The sequence parameters are listed in Table 1.

A reference image of the phantom was obtained before placement of any aneurysm clip. Each clip was then scanned with each pulse sequence, with the clip placed in one of two different orientations: once with the long axis parallel to the static magnetic field, and once with the long axis perpendicular to the static magnetic field (Fig. 2 C, D). The phantom was placed inside in the head coil,

Table 1. Imaging parameters

Sequence	3D ZTE	3D T2W FSE	3D T1WI SPGR	3D T2*W SPGR	2D DWI with SE-EPI
Number of slices	128	132	1132	132	64
FOV (cm)	25.6	25.6	25.6	25.6	25.6
TR (ms)	49.728	3000	6.328	30	10000
TE (ms)	0.016	72.283	1.832	15	76.9
BW (Hz/pixel)	3906.25	651.016	325.547	325.547	3906.25
Frequency sampling point	128	256	256	256	64
Phase matrix sampling point	128	256	256	256	128
Slice thickness (mm)	2	1	1	1	2
Slice gap (mm)	0	0	0	0	0
Image matrix size	512	512	512	512	512
Averages	1	1	1	1	2
Flip angle (degrees)	4	90	15	20	90
Acceleration factor of parallel imaging	1	slice: 2, phase: 2	2	1	2

3D, three-dimensional; ZTE, zero echo time; SPGR, spoiled gradient recalled acquisition in the steady state; T2*W, T2*-weighted; 2D, two-dimensional; FOV, field of view; TR, repetition time; TE, echo time; BW, bandwidth.

the clip was positioned at the isocenter of the static magnetic field, and the phantom was scanned sagittally to the static magnetic field. For all MR images, the frequency direction was always parallel to the static magnetic field.

4. Assessing Clip Artifacts

Clip artifact was determined according to the ASTM-F2119-07 standard.

In each image, the magnitude of the clip artifact was automatically calculated on a pixel-by-pixel or voxel-by-voxel basis using in-house software, as follows: 100 (%) × (intensity in the image with the clip – intensity in the reference image) / intensity in the reference image. A voxel or pixel was defined as having artifact when the absolute value of the calculated value was >30%, and voxels or pixels with these artifacts were automatically displayed using the same in-house software mentioned above (Fig. 3). For artifact distance, a line parallel to the static magnetic field was automatically determined on each image containing a clip and this baseline was automatically transferred to the corresponding artifact image (Fig. 3). A line parallel to the baseline was then manually determined on each artifact image so that the line was located at the center of the artifact (Fig. 3). The number of pixels affected by artifact was automatically counted on the center line using Image J (ver.1.50f; National Institutes of Health, Bethesda, MD, USA), and the number of pixels was then manually converted to the distance. When the long axis of the clip was set parallel to the static magnetic field, artifact distance (mm) was manually calculated as follows: (converted distance – length of the clip)/2 [16-18]. When the long axis of the clip was set perpendicular to the static magnetic field, artifact distance (mm) was manually calculated as follows: (converted distance – width of the

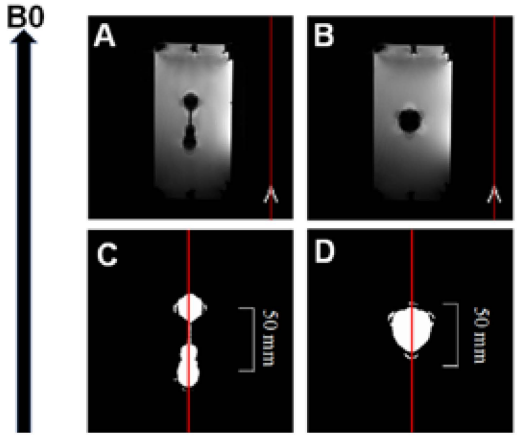

Fig. 3. Top-view images of artifact produced by the long straight clip (No. 92) on three-dimensional T2*-weighted imaging with spoiled gradient recalled acquisition in the steady state technique. The long axis of the clip is oriented parallel (A) or perpendicular (B) to the static magnetic field. A line parallel to the static magnetic field is automatically determined on each image with a clip (red lines on A and B). On each artifact image (C, D), a line parallel to the baseline is transferred from the upper image (A, B) such that this line is located at the center of the artifact (red lines).
B0, static magnetic field.

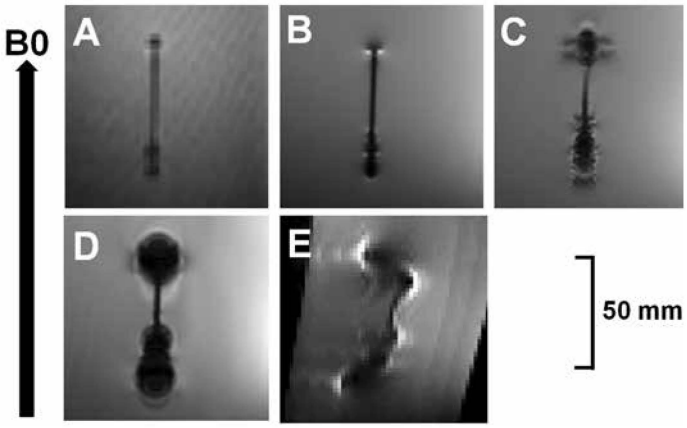

Fig. 4. Magnetic resonance images of the long straight clip (No. 92) obtained with each of the five pulse sequences. The long axis of the clip is set parallel to the static magnetic field. A. Three-dimensional zero time-of-echo imaging. B. three-dimensional T2-weighted fast spin echo imaging. C. three-dimensional T1-weighted imaging with spoiled gradient recalled acquisition in the steady state technique. D. three-dimensional T2*-weighted imaging spoiled gradient recalled acquisition in the steady state technique. E. two-dimensional diffusion-weighted imaging acquired with spin-echo echo-planar imaging. On the last sequence, the artifact extends beyond the edge of the phantom.
B0, static magnetic field.

clip)/2 [16].

For artifact volume, the number of voxels with artifacts was automatically counted using Image J on each artifact image and then manually converted to the volume. Artifact volume (mm^3) was manually calculated as follows: converted volume – volume of the clip.

5. Statistical Analyses

Data are expressed as means ± standard deviation (SD). The artifact distance and volume among four or five groups were compared using repeated measures analysis of variance followed by Fisher's PLSD test. The artifact distance and volume between two groups were compared using Wilcoxon signed rank test. For all statistical analyses, significance was set at the $p < 0.05$ level.

III. Results

For four of the five pulse sequences, artifact distance and artifact volume could be calculated for all five of the tested aneurysm clips (Fig. 4 A-D). On 2D DWI with SE-EPI, however, artifact extended beyond the phantom for all five clips (Fig. 4 E) and therefore no artifact distances or artifact volumes could be calculated for this sequence.
Table 2 shows the artifact distance for each

Table 2. Results of artifact distance

Type of clip	Short straight (No. 2)	Right-angled (No. 22)	Straight fenestrated (No. 30)	45° -angled (No. 49)	Long straight (No. 92)	Mean ± SD
Clip orientation to B0	Para.	Para.	Para.	Para.	Para.	
3D ZTE	2.85	3.50	3.70	3.55	4.00	3.5 ± 0.4
3D T2W FSE	3.35	3.25	3.20	4.33	4.25	3.7 ± 0.6
3D T1WI SPGR	7.35	5.00	7.20	5.55	9.00	6.8 ± 1.6
3D T2*W SPGR	8.10	9.25	8.45	10.80	11.00	9.5 ± 1.3
Mean ± SD	5.4 ± 2.7	5.3 ± 2.8	5.6 ± 2.6	6.1 ± 3.3	7.1 ± 3.5	
Clip orientation to B0	Perpen.	Perpen.	Perpen.	Perpen.	Perpen.	
3D ZTE	3.90	5.35	5.15	5.10	6.70	5.2 ± 1.0
3D T2W FSE	4.65	5.15	6.15	4.65	6.20	5.4 ± 0.8
3D T1WI SPGR	6.90	9.35	7.65	6.65	10.45	8.2 ± 1.6
3D T2*W SPGR	11.15	12.15	16.15	11.60	14.70	13.2 ± 2.2
Mean ± SD	6.7 ± 3.3	8.0 ± 3.4	8.8 ± 5.0	7.0 ± 3.2	9.5 ± 3.9	

B0, static magnetic field; Para, parallel to B0; Perpen, perpendicular to B0; 3D, three-dimensional; ZTE, zero echo time; SPGR, spoiled gradient recalled acquisition in the steady state; T2*W, T2*-weighted; 2D, two-dimensional; N.C., not calculated.
Values are expressed as mm.

of the tested clips, for each pulse sequence. This value was significantly longer on 3D T2*W SPGR than on 3D ZTE ($p < 0.0001$ for setting parallel to the static magnetic field; $p < 0.0001$ for setting perpendicular to the static magnetic field), 3D T2W FSE ($p < 0.0001$ for setting parallel to the static magnetic field; $p < 0.0001$ for setting perpendicular to the static magnetic field) or 3D T1W SPGR ($p = 0.0007$ for setting parallel to the static magnetic field; $p < 0.0001$ for setting perpendicular to the static magnetic field). It was also significantly longer on 3D T1W SPGR than on 3D ZTE ($p = 0.0001$ for setting parallel to the static magnetic field; $p = 0.0008$ for setting perpendicular to the static magnetic field) or 3D T2W FSE ($p = 0.0002$ for setting parallel to the static magnetic field; $p = 0.0010$ for setting perpendicular to the static magnetic field). However, the artifact distance did not differ between 3D ZTE and 3D T2W FSE despite the direction on which the long axis of the clip was set to the static magnetic field. Artifact distance was significantly longer when the long axis of the clip was set perpendicular to the static magnetic field than when it was set parallel to the static magnetic field ($p = 0.0431$ for 3D ZTE, 3D T2W FSE and 3D T2*W SPGR), except for 3D T1WI SPGR.

When the long axis of each clip was set parallel to the static magnetic field and artifact distance was compared among the clips, the value of the long straight clip was significantly longer than that of the short straight ($p = 0.0296$) or right-angled ($p = 0.0190$) clip (Table 2).When the long axis of each clip was set perpendicular to the static magnetic field, the artifact distance of the short straight clip was significantly shorter than that of the straight fenestrated ($p = 0.0139$) or long straight (p

Table 3. Results of artifact volume

Type of clip	Short straight (No. 2)	Right-angled (No. 22)	Straight fenestrated (No. 30)	45° -angled (No. 49)	Long straight (No. 92)	Mean ± SD
Clip orientation to B0	Para.	Para.	Para.	Para.	Para.	
3D ZTE	233	967	878	510	1510	820 ± 485
3D T2W FSE	1586	4001	2797	2967	4394	3149 ± 1104
3D T1WI SPGR	5280	10725	7103	8230	14589	9185 ± 3608
3D T2*W SPGR	24683	38278	29666	33519	54896	36208 ± 11580
Mean ± SD	7946 ± 11360	13493 ± 17019	10111 ± 13294	11307 ± 15154	18847 ± 24679	
Clip orientation to B0	Perpen.	Perpen.	Perpen.	Perpen.	Perpen.	
3D ZTE	1093	1627	1551	1774	10275	3264 ± 3928
3D T2W FSE	4680	6311	6719	6592	26031	10067 ± 8962
3D T1WI SPGR	9767	12591	13392	13022	42650	18284 ± 13696
3D T2*W SPGR	37131	48163	52529	49720	167708	71050 ± 54349
Mean ± SD	13168 ± 16367	17173 ± 21143	18548 ± 23167	17777 ± 21788	61666 ± 71920	

B0, static magnetic field; Para, parallel to B0; Perpen, perpendicular to B0; 3D, three-dimensional; ZTE, zero echo time; SPGR, spoiled gradient recalled acquisition in the steady state; T2*W, T2*-weighted; 2D, two-dimensional; N.C., not calculated.
Values are expressed as mm^3.

= 0.0022) clip (Table 2). The value of the 45° -angled clip was also significantly shorter than that of the straight fenestrated (p = 0.0333) or long straight (p = 0.0053) clip (Table 2).

Table 3 lists the artifact volumes for all aneurysm clips tested, for each pulse sequence. This value was significantly greater on 3D T2*W SPGR than on 3D ZTE (p < 0.0001 for setting parallel to the static magnetic field; p = 0.0006 for setting perpendicular to the static magnetic field), 3D T2W FSE (p < 0.0001 for setting parallel to the static magnetic field; p=0.0013 for setting perpendicular to the static magnetic field) and 3D T1W SPGR (p = 0.0007 for setting parallel to the static magnetic field; p = 0.0036 for setting perpendicular to the static magnetic field). The artifact volume did not differ among other pulse sequences despite the direction on which the long axis of the clip was set to the static magnetic field. Artifact volume was significantly greater in clips with their long axes set perpendicular to the static magnetic field than in those set parallel to the static magnetic field on all four pulse sequences (p = 0.0431).

When the long axis of each clip was set parallel to the static magnetic field and the artifact volumes for the five clips were compared, the value of the long straight clip was significantly greater than that of the short straight (p = 0.0112) or straight fenestrated (p = 0.0336) clip (Table 3). When the long axis of each clip was set perpendicular to the static magnetic field, the artifact volume of the long straight clip was significantly greater than that of the short straight (p = 0.0117), right-angled (p = 0.0184), straight fenestrated (p = 0.0216) or 45° -angled clip (p = 0.0198) (Table 3). Regarding the relationship between the magnitude of the artifact and specific parts

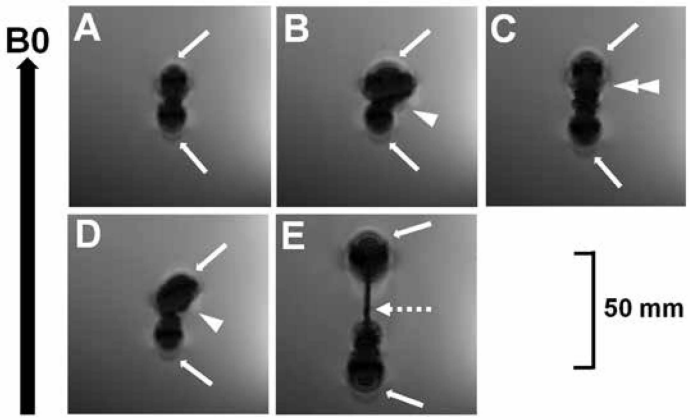

Fig. 5. Magnetic resonance images of the five clip types on three-dimensional T2*-weighted imaging with spoiled gradient recalled acquisition in the steady state technique. The long axis of each clip is oriented parallel to the static magnetic field. For all five clip types, there is prominent development of artifact at both ends of the clip (white arrows) that is also seen at curved (single white arrowhead) and fenestrated (double white arrowheads) portions. In contrast, artifact is minimal at the middle of the blade of the clip (white dotted arrow). The clips shown in A, B, C, D or E are the same as those shown in Figure 1.
B0, static magnetic field

of the aneurysm clip, there was prominent development of artifact at both ends of the clip (Fig. 5) for all five types of clip. There was also prominent development of artifact at the curved or fenestrated portion of the clip (Fig. 5B, C and D). In contrast, artifact was minimal at the mid-part of the blade when the clip was set parallel to the static magnetic field (Fig. 5E).

IV. Discussion

The present study showed the following findings: first, susceptibility artifacts produced by titanium alloy aneurysm clips on 7T MR were greater on 3D T2*W SPGR than on other pulse sequences except 2D DWI, the artifacts on 3D ZTE were equivalent to those on 3D T2W FSE and the artifacts on these two sequences were less than those on other sequences; second, the susceptibility artifacts were greater on the long straight clip than other clips; and third, whereas there was prominent development of artifact at both ends, at the curved or fenestrated portion of the clip, artifact was minimal at the mid-part of the blade.

Spin echo techniques such as 3D T2W FSE use the 180° pulse to refocus the spins, thereby minimizing the effects of the local field distortion. Gradient echo techniques such as 3D T1W SPGR and 3D T2*W SPGR do not have this pulse, so the image distortion is worse 17,18. Thus, susceptibility artifacts are more pronounced using the latter than the former [17, 18]. Our data corresponded with these theories.

Susceptibility artifacts on 2D DWI were so great that they exceeded the phantom and their magnitudes could not be calculated. This imaging generally suffers from geometric

distortions since it takes a relatively longer sampling interval to collect the data in the phase-encoding direction [19, 20]. In particular, these distortions become greater under existence of metals. This sequence should be applied for 1.5T or 3T MRI rather than 7T MRI in patients undergoing aneurysmal clipping.

The artifact distance on 3D ZTE was equivalent to that on 3D T2W FSE and these values on these two sequences were shorter than those on other sequences. The novel 3D ZTE sequence is often used for MRA [21-23]. Susceptibility artifacts theoretically increase as echo time lengthens [24, 25]. This explains why artifact volume was lower on 3D ZTE than on other sequences, because the echo time on 3D ZTE is approximately zero. Several investigators have recently showed that MRA with 3D ZTE is superior to that with 3D time-of-flight (TOF) for visualizing the parent artery and assessing occlusion status in patients undergoing coil embolization or flow-diverter placement for cerebral aneurysms [26, 27]. Compared with 3D TOF-MRA, 3D ZTE-MRA provides more accurate aneurysm diameter measurement, especially in smaller aneurysms, which enables better depiction of remnant treated aneurysm or recurrence [21-23]. Interobserver agreement for stenosis grading of intracranial main arteries is reportedly higher for 3D ZTE-MRA than 3D TOF-MRA due to higher signal homogeneity, higher venous signal suppression, and lower susceptibility to field inhomogeneity21). Further, artifacts due to turbulent blood flow may be minimized [23,27] and acoustic noise is reduced [21,28] in 3D ZTE-MRA. Considering these findings and our data, 3D ZTE-MRA on 7T MRI will be used to assess clipped aneurysms and subsequent de novo aneurysms in detail.

Susceptibility artifacts are theoretically produced by large differences in magnetic susceptibility between the metallic object and the surrounding matter [24], and are minimized when the long axis of the object is parallel to the direction of the static magnetic field [25]. In contrast, they are strongly produced in the boundary between the metallic object and the surrounding matter when this boundary is perpendicular to the direction of the static magnetic field: the longer or larger the boundary line or surface, respectively, the greater the susceptibility artifac [25]. These theories explain our finding that the magnitudes of susceptibility artifacts were greater when the long axes of aneurysm clips were set perpendicular to the static magnetic field than when set parallel to the static magnetic field. They also explain why susceptibility artifact was so extensive for the long straight clip despite the direction of the long axis of an aneurysmal clip to the static magnetic field, which was another finding of our study. Among the five types of tested clips, the long straight clip has the greatest length, width, and volume, and therefore the boundary line or surface between the metallic object and the surrounding matter that is perpendicular to the direction of the static magnetic field is greatest for this aneurysm clip. In contrast, susceptibility artifact was less for the short straight clip than for the right-angled clip, 45° -angled clip, and straight fenestrated clip. The volume of the short straight clip is lower than that of these other three clips, even though they all have the same

width. In addition, susceptibility artifact was prominent around sections with a complicated shape, such as a curve or fenestration, but was minimal around straight sections. These findings are explained as follows: the boundary surface area between the metallic object and the surrounding matter that is perpendicular to the direction of the static magnetic field is greater for a section with a complicated shape than a straight section. These findings suggested that use of the shorter and more simply/shaped on clipping for a cerebral aneurysm is better from the viewpoint of susceptibility artifact.

This study does have some limitations. Because the ASTM does not request confirmation of reproducibility for measuring susceptibility artifact, we measured the artifact only one time for each clip on each pulse sequence. The static magnetic field is not always uniform. Therefore, confirmation of the reproducibility would be beneficial. We also measured susceptibility artifact when the long axis of each clip was set parallel or perpendicular to the static magnetic field. This is another limitation. Aneurysm clips are set with various degree to the static magnetic field in clinical settings. Our data may not be applicable for conditions except aneurysm clips set parallel or perpendicular to the static magnetic field.

V. Conclusion

Susceptibility artifacts produced by titanium alloy aneurysm clips on 7T MR were greater on 3D T2*W SPGR than on other pulse sequences except 2D DWI, the artifacts on 3D ZTE were equivalent to those on 3D T2W FSE and the artifacts on these two sequences were less than those on other sequences. The susceptibility artifacts were greater on the long straight clip than other clips. Whereas there was prominent development of artifact at both ends, at the curved or fenestrated portion of the clip, artifact was minimal at the mid-part of the blade.

Conflict of interest: The authors have no conflict of interest to declare.

References

1) **Grandin CB, Cosnard G, Hammer F, et al.**: Vasospasm after subarachnoid hemorrhage: diagnosis with MR angiography. Am J Neuroradiol **21**, 1611-16171, 2000.
2) **De Cocker LJ, Lindenholz A, Zwanenburg JJ, et al.**: Clinical vascular imaging in the brain at 7T. Neuroimage **168**, 452-458, 2018.
3) **Wrede KH, Matsushige T, Goericke SL, et al.**: Non-enhanced magnetic resonance imaging of unruptured intracranial aneurysms at 7 Tesla: Comparison with digital subtraction angiography. Eur Radiol **27**, 354-364, 2017.
4) **von Morze C, Xu D, Purcell DD, et al.**: Intracranial time-of-flight MR angiography at 7T with comparison to 3T. J Magn Reson Imaging **26**, 900-904, 2007.
5) **Matsushige T, Kraemer M, Schlamann M, et al.**: Ventricular Microaneurysms in Moyamoya Angiopathy Visualized with 7T MR Angiography. Am J Neuroradiol **37**, 1669-16723, 2016.
6) **Wrede KH, Dammann P, Monninghoff C, et al.**: Non-enhanced MR imaging of cerebral aneurysms: 7 Tesla versus 1.5 Tesla. PLoS One **9**, e84562, 2014.
7) **Gönner F, Lövblad KO, Heid O, et al.**: Magnetic resonance angiography with ultrashort echo

times reduces the artefact of aneurysm clips. Neuroradiology **44**, 755-758, 2002.

8) **Dula AN, Virostko J** and **Shellock FG**: Assessment of MRI issues at 7 T for 28 implants and other objects. Am J Roentgenol **202**, 401-405, 2014.

9) **Hoff MN, McKinney At, Shellock FG, et al.**: Safety Considerations of 7-T MRI in Clinical Practice. Radiology **292**, 509-518, 2019.

10) **Matsuura H, Inoue T, Konno H, et al.**: Quantification of susceptibility artifacts produced on high-field magnetic resonance images by various biomaterials used for neurosurgical implants. Technical note. J Neurosurg **97**, 1472-1475, 2002.

11) **Singleton RH, Kellermier H** and **Lunsford LD**: Radiation-induced meningioma concealed by shunt valve artifact: case report. Neurosurgery **62**, E743-744, 2008.

12) **Matsuura H, Inoue T, Ogasawara K, et al.**: Quantitative analysis of magnetic resonance imaging susceptibility artifacts caused by neurosurgical biomaterials: comparison of 0.5, 1.5, and 3.0 Tesla magnetic fields. Neurol Med Chir (Tokyo) **45**, 395-399, 2005.

13) **Olsrud J, Latt J, Brockstedt S, et al.**: Magnetic resonance imaging artifacts caused by aneurysm clips and shunt valves: dependence on field strength (1.5 and 3 T) and imaging parameters. J Magn Reson Imaging **22**, 433-437, 2005.

14) American Society for Testing and Materials (ASTM) International: F2119-07 Test method for evaluation of MR image artifacts from passive implants. American Society for Testing and Materials (ASTM) International, West Conshohocken, PA2013.

15) **Jackson E, Bronskill M, Drost D, et al.**: Acceptance testing and quality assurance procedures for magnetic resonance imaging facilities. Report No. 101, American Association of Physicists in Medicine, 2010.
https://doi.org/10.37206/101

16) **Chiba Y, Murakami H, Sasaki M, et al.**: Quantification of metal-induced susceptibility artifacts associated with ultrahigh-field magnetic resonance imaging of spinal implants. JOR Spine **2**, e1064, 2019.

17) **Lee MJ, Kim S, Lee SA, et al.**: Overcoming artifacts from metallic orthopedic implants at high-field-strength MR imaging and multi-detector CT. Radiographics **27**, 791-803, 2007.

18) **Port JD** and **Pomper MG**: Quantification and minimization of magnetic susceptibility artifacts on GRE images. J Comput Assist Tomogr **24**, 958-964, 2000.

19) **Techavipoo U, Lackey J, Shi J, et al.**: Phase labeling using sensitivity encoding (PLUS): data acquisition and image reconstruction for geometric distortion correction in EPI. Magn Reson Med **61**, 650-658, 2009.

20) **Yarach U, In MH, Chatnuntawech I, et al.** : Model-based iterative reconstruction for single-shot EPI at 7T. Magn Reson Med **78**, 2250-2264, 2017.

21) **Shang S, Ye J, Dou W, et al.**: Validation of Zero TE-MRA in the Characterization of Cerebrovascular Diseases: a feasibility study. Am J Neuroradiol **40**, 1484-1490, 2019.

22) **Song Y, Qi P, Huang J, et al.**: Application of zero echo time MR angiography in follow-up of intracranial aneurysm remnant and in-stent lumen after embolization: a comparison study with digital subtraction angiography. Acta Radiol **61**, 480-486, 2019.

23) **Takano N, Suzuki M, Irie R, et al.**: Usefulness of Non-Contrast-Enhanced MR Angiography Using a Silent Scan for Follow-Up after Y-Configuration Stent-Assisted Coil Embolization for Basilar Tip Aneurysms. Am J Neuroradiol **38**, 577-581, 2017.

24) **Lee MJ, Kim S, Lee SA, et al.**: Overcoming artifacts from metallic orthopedic implants at high-field-strength MR imaging and multi-detector CT. Radiographics **27**, 791-803, 2007.

25) **Port JD** and **Pomper MG**: Quantification and minimization of magnetic susceptibility artifacts on GRE images. J Comput Assist Tomogr **24**, 958-964, 2000.

26) **Irie R, Suzuki M, Yamamoto M, et al.**: Assessing blood flow in an intracranial stent: a feasibility study of MR angiography using a silent scan after stent-assisted coil embolization for anterior circulation aneurysms. Am J Neuroradiol **36**, 967-970, 2015.

27) **Oishi H, Fujii T, Suzuki M, et al.**: Usefulness of silent MR angiography for intracranial aneurysms Treated with a flow-diverter device. Am J Neuroradiol **40**, 808-814, 2019.

28) **Larson PEZ, Han M, Krug R, et al.**: Ultrashort echo time and zero echo time MRI at 7T. Magma (New York) **29**, 359-370, 2016.

岩手医誌 73 巻，5 号（令和 3 年 12 月）215-226 頁.

7 テスラ MRI 上にチタン合金製動脈瘤クリップが作る磁気アーチファクトの定量

筒井章太[1)]，松田　豪[2)]，武田航太[2)]，
佐々木真理[2)]，藤本健太郎[1)]，柳原　晋[1)]，
幸治孝裕[1)]，久保慶高[1)]，小笠原邦昭[1)]

[1)] 岩手医科大学医学部，脳神経外科学講座
[2)] 岩手医科大学医歯薬総合研究所，超高磁場 MRI 診断・病態研究部門

(Received on January 14, 2021 & Accepted on February 12, 2021)

要旨

脳動脈瘤をもつ症例では，開頭クリッピング後にしばしば MRI を撮像する．本研究の目的は，7T MRI 上種々の形状のチタン合金製動脈瘤クリップが作る磁気アーチファクトの大きさを種々の撮像法で定量することであった．短い，長い，まっすぐ，曲がりあるいは有窓の組み合わせからなる５つの異なる形状の動脈瘤クリップを植物オイルで満たしたファントムに入れ，５つの異なる撮像法で撮像した．アーチファクトを含むピクセルあるいはボクセルを決定し，アーチファクト距離･体積を算出した．アーチファクト距離･体積は他の撮像法に比して 3D T2*-weighted with spoiled gradient recalled acquisition in the steady state imaging が大きく，3D zero time-of-echo が小さかった．各クリップ間では，長い直のクリップのアーチファクト距離・体積が最大であった．どのクリップにおいても，両端，曲がり，有窓部はまっすぐな部分よりアーチファクトが大きかった．